Chapter 11
The Confinement and Migration of Charge-Carriers in Lead Halide Perovskites

Sushant Ghimire, Lata Chouhan, and Vasudevanpillai Biju

Abstract With the growing success of halide perovskites as functional materials in solar cells, LEDs, and lasers, studies are progressing to reveal their optical and charge-carrier properties. This chapter describes the consequences of charge-carrier generation, stabilization, and recombination in perovskite nanocrystals, quantum dots, and their assemblies. The strong confinement of charge-carriers in perovskite quantum dots causes photoluminescence blinking with distinct ON and OFF events, which is due to photocharging and ultrafast Auger nonradiative recombination. Such a blinking with long OFF periods suppresses superoxide generation and oxidation of perovskites. When perovskite nanocrystals and quantum dots are closely-packed into superlattices, the carrier confinement is broken due to the narrowing of inter-particle energy levels and the formation of minibands that allow for carrier migration. This results in unexpectedly delayed photoluminescence at low intensities of excitation light, whereas at high intensities of excitation light, the ultrafast radiative recombination of charge-carriers occurs. These properties of quantum dots, nanocrystals, and assemblies of perovskites are important to be considered during the construction of devices such as solar cells, LEDs, and lasers.

Keywords Halide perovskites · Nanocrystals · Quantum dots · Perovskite assemblies · Single particle studies

Sushant Ghimire and Lata Chouhan: Equal contribution.

S. Ghimire · L. Chouhan · V. Biju
Graduate School of Environmental Science, Hokkaido University, N10, W5, Sapporo, Hokkaido 060-0810, Japan
e-mail: ghimiresushant@eis.hokudai.ac.jp

V. Biju (✉)
Research Institute for Electronic Science, Hokkaido University, N20, W10, Sapporo, Hokkaido 001-0020, Japan
e-mail: biju@es.hokudai.ac.jp

11.1 Introduction

Halide perovskites are exciting materials for light-harvesting [1–3] and light-emitting [4–6] applications. Their success foots on the large absorption coefficient, high charge-carrier mobility, high photoluminescence (PL) quantum yield (QY), and cost-effective synthesis [1–6]. Further, the emission color from halide perovskites can cover the entire UV-visible-near infrared spectrum, which emanates from different band-gaps induced by changing the halogen compositions in the material [4–6]. Interestingly, these properties of halide perovskite are maintained irrespective of their size. Such attributes make halide perovskites highly promising semiconductor materials that can compete with the existing silicon technology for solar cells and quantum dot (QD) technology for light-emitting devices and displays. In addition to the chemical and physical stability of perovskites, the generation, stabilization, and binding energy of charge-carriers in these materials are also fundamental aspects to be considered for such device applications.

Charge-carrier dynamics in halide perovskites are complicated by the coexistence of bound electron-hole pairs (excitons) and free charge-carriers [7–11]. The coulombic binding between an electron and a hole in an exciton can be strong or weak, depending upon the exciton binding energy (E_b). Weakly and strongly bound excitons in semiconductors are shown schematically in Fig. 11.1. Weakly bound excitons are called Mott-Wannier excitons (Fig. 11.1a), where low E_b results in the larger delocalization of electron-hole pair, resulting in exciton Bohr radius (R_B) much greater than the lattice constant (a) of the material. On the other hand, strongly bound
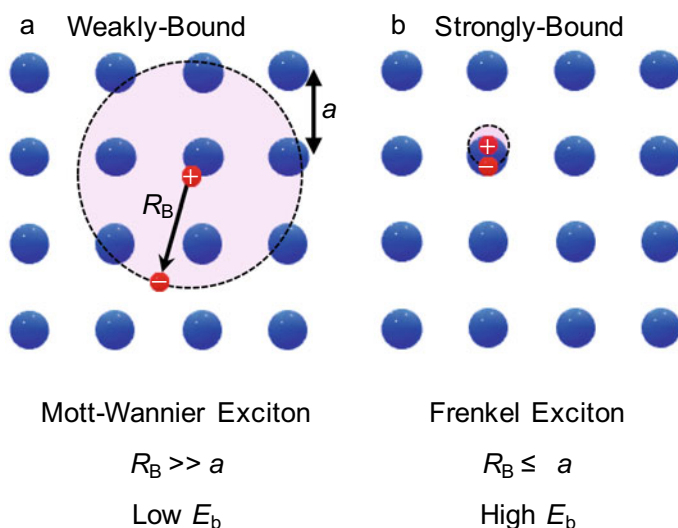
Fig. 11.1 Weakly and strongly bound excitons in semiconductors. **a** Mott-Wannier type and **b** Frenkel type excitons, where R_B is exciton Bohr radius, a is lattice constant, and E_b is exciton binding energy

exciton with high E_b is called Frenkel exciton whose R_B is much smaller than the a of the material (Fig. 11.1b). In halide perovskites, E_b lies in between those of Mott-Wannier and Frenkel excitons and is either less than or comparable to the thermal energy. Hence, free charge-carriers dominate in the films and bulk single crystals of these materials. Studies have shown that the free charge-carriers are the consequence of dissociation of excitons when the associated binding energy is overcome by the thermal energy [8–12]. The free charge-carrier property of halide perovskites is associated with long carrier diffusion lengths and lifetimes, as observed in the case of bulk films and single crystals [2, 3]. Nevertheless, the carrier lifetime varies in the range of sub-nanoseconds to microseconds in different types of halide perovskites, depending upon their size, dimensionality, and composition [2, 3, 8–15].

Exciton binding energies in perovskite nanocrystals (PNCs) are higher than the corresponding bulk crystal. For example, E_b of 320 meV is reported for MAPbBr$_3$ (MA = methylammonium, $CH_3NH_3^+$) nanocrystals, which is more than three times higher (84 meV) than that for the corresponding bulk crystal [16]. Therefore, quantum confinement effects are observed in PNCs as well, when their physical size becomes smaller than the corresponding R_B values [13, 15]. Additionally, the quantum confinement effects in PNCs are depended upon not only the size but also the dimensionality. For instance, blue-shift in absorption and PL spectra, which is associated with the increase in optical band-gap, is observed in the case of perovskite nanoplatelets when the layer thickness decreases below R_B [15]. Despite the quantum confinement effects in PNCs, when compared to the conventional chalcogenide QDs, slow cooling and efficient extraction of hot carriers are reported in their colloidal solutions [17]. The intrinsic phonon bottleneck and Auger heating effects at low and high carrier densities, respectively, in PNCs account for such observations. Apart from this, the excellent optoelectronic properties of PNCs, which are comparable to the conventional QDs, are maintained even at the weak quantum confinement regime. While R_B in lead halide perovskites lies in the range of 2–7 nm [13, 15, 16, 18, 19], most of the studies demonstrating the light-emitting [4, 6] and photovoltaic [17, 18] applications of PNCs show the nanocrystal size either only slightly smaller or larger than the corresponding R_B value. This suggests that, compared to the chalcogenide QDs, the application of PNCs in light-harvesting and light-emitting device is diverse and immense.

11.2 Photoluminescence Blinking

In quantum-confined semiconductor nanocrystals or QDs, the photogenerated electrons and holes are strongly correlated. Carrier dynamics in such strongly confined QDs is governed by the discrete energy states showing sharp excitonic band in the absorption spectrum, fast radiative recombination of charge-carriers, carrier multiplication or multi-exciton generation, and increased Auger recombination [20]. Moreover, the PL properties of these semiconductor nanocrystals at their single particle level are often intricated by the stochastic emission behavior with a sequence of bright

'ON' and dark 'OFF' events known as PL intermittency or blinking. This is attributed to the random charging by photoionization and neutralization or discharging of the QD. The blinking behavior in QDs is often described as A-type and B-type [21]. In A-type blinking, the 'OFF' state is associated with the decrease in PL lifetime, whereas the carrier-recombination rates are not affected by the 'OFF' or the 'ON' states in B-type blinking. The short PL lifetime observed during the 'OFF' state in A-type blinking is attributed to the formation of a charged excitonic state called a trion (X^-) which promotes the mono-exponential nonradiative Auger-type carrier recombination in QDs. On the other hand, B-type blinking mostly depends on the activation and deactivation of the traps or its recombination centers which leads to the 'ON' and 'OFF' states, respectively.

Apart from the QDs, diverse stochastic emission behavior has been observed in the case of perovskite single nanocrystals, microcrystals, and thin films [22–27]. Some perovskite single-emitters have shown blinking with two-state fluctuations between 'ON' and 'OFF' events [24, 25, 27], which is similar to the case of chalcogenide QD and is ascribed to the process of photocharging and neutralization. Semiconductor nanocrystals or QDs show various interesting optoelectronic properties in the isolated forms. On the other hand, multi-state PL blinking has also been reported from the nanocrystals, microcrystals, and films of lead halide perovskite [22, 23, 26]. An early report on PL blinking in MAPbI$_3$ PNCs and microcrystals has shown that the chemical and structural properties of material are responsible for the multi-state stochastic emission behavior [22]. This is explained through two mechanisms, namely the quenching-site and the emitting-site model, which is shown in Fig. 11.2. In emitting-site model, as shown in Fig. 11.2a, the emitters are at the either end of the nanocrystal which randomly get charged and discharged leading to the 'ON' and 'OFF' states, respectively. Quenching-site model (Fig. 11.2b) considers the whole nanocrystal as an emissive site, where the emission localization position and center of the nanocrystals lie at the same point. Quenchers in quenching-site model act as traps which are present at the either end of the nanocrystal and deactivate the electrons and holes during the diffusion, resulting in the 'OFF' state. An interesting behavior of PL blinking in lead halide perovskites is that, unlike lead chalcogenide QDs, the multi-state PL fluctuations in these semiconductor materials is suppressed under high-intensity of excitation, which on the other hand becomes more intense at low-intensity of excitation. Figure 11.3a shows the excitation laser intensity-dependent PL blinking in MAPbI$_3$ PNCs at the ambient environment. The suppression of PL blinking in such perovskite samples at high-intensity excitation is attributed to the decrease in efficiency of active quenchers to trap large number of charges. Alternately, more emitting sites are generated at high-intensity excitation, resulting in the averaged PL intensity over many emitting sites. Nevertheless, as shown in Fig. 11.3a(i) and b(i), photobleaching cannot be ruled out at high-intensity excitation under the ambient atmosphere [22, 25, 27].
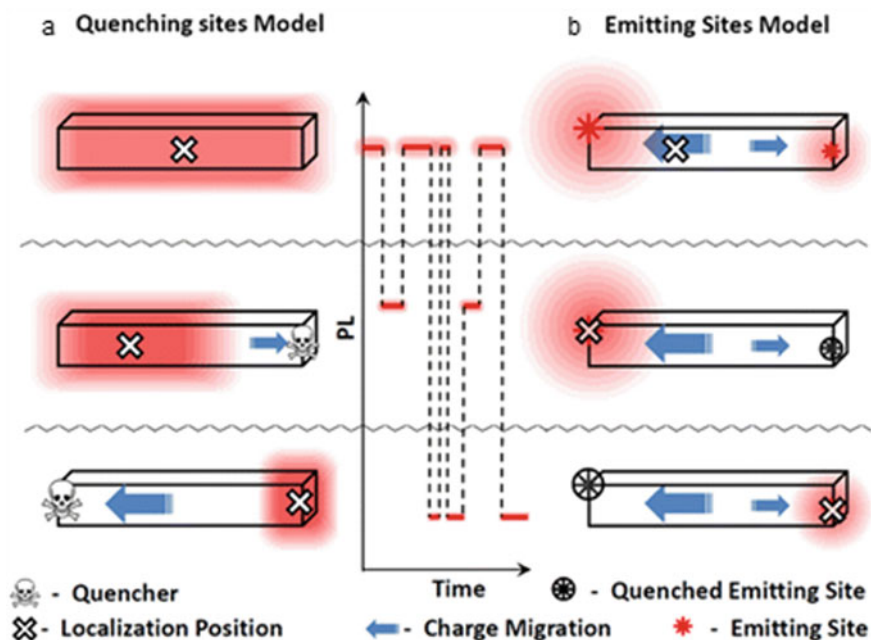
Fig. 11.2 Models of PL blinking in lead halide perovskites: **a** Quenching-site model and **b** emitting-site model. Reproduced with permission from Ref. [22]. Copyright 2015, American Chemical Society

11.3 External Factors Affecting the Photoluminescence

Importantly, different environmental factors such as moisture, nitrogen, oxygen, polymer, and light have shown variable results on the PL properties of perovskites at their single particle level [24, 27]. The PL blinking trajectories of $MAPbI_3$ nanocrystals at different local environment are shown in Fig. 11.3b. For example, different roles of oxygen on the PL properties of lead halide perovskites have been reported for different types of perovskite samples [22, 25, 27]. While PL brightening was observed as the consequence of photoinduced trap-filling in the case of $MAPbI_3$ PNCs in presence of oxygen [22], PL bleaching was reported in $CsPbI_3$ perovskite QDs under the similar environment [27]. Recently, a study carried out at the single particle level in $MAPbI_3$ PNCs under air, argon, and polymer matrix (Fig. 11.3b) reveals its PL degradation mechanism [25]. The PNCs degrade or photobleach under the air atmosphere, whereas the PL intensity remains constant under the argon and the polymer atmosphere. The photostability of a PNC under the argon or the polymer atmosphere is the result of low reactivity of oxygen with the nanocrystal during its 'ON' state. Interestingly, as shown in Fig. 11.3b(iv), a recovery of PL intensity level is observed even at the air atmosphere after the long 'OFF' event, suggesting that there
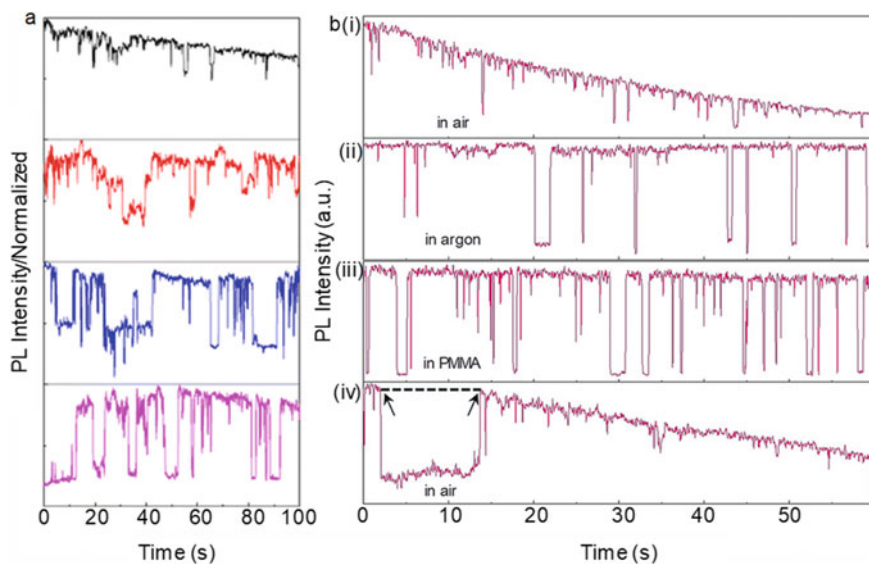
Fig. 11.3 Excitation intensity- and local environment-dependent PL blinking in lead halide perovskites. **a** PL blinking in MAPbI$_3$ PNCs under increasing intensity of the excitation laser: (bottom) 0.01 to (top) 0.5 Wcm^{-2}. **b** PL blinking in MAPbI$_3$ PNCs (i, iv) in air (ii) under continuous argon purging, and (iii) in polymer matrix Reproduced with permission: (**a**) from Ref. [22]. Copyright 2015, American Chemical Society. (**b**) From Ref. [25]. Copyright 2019, Wiley-VCH

was no degradation of PNCs during the long 'OFF' duration that involves nonradiative recombination. Alternately, the PL degradation at the air atmosphere when the PNCs were more frequently in the 'ON' state or with the long-living 'ON' duration can be ascribed to the oxidation of nanocrystals by the generation of superoxide, which is discussed schematically in Fig. 11.4. Here, the neutral and ionized states are responsible for the 'ON' and 'OFF' events in the PL blinking trajectories of PNCs. When the nanocrystal is in excited state, it can either oxidize and transfer electron to the oxygen present in the atmosphere generating superoxide or get ionized. The generated superoxide can take the vacancies of the anion and deprotonate the methyl ammonium cation, thereby slowly degrading the PNCs. On the other hand, when the nanocrystal is in the ionized state, nonradiative recombination becomes faster than the electron transfer, and the reactivity of oxygen is suppressed during the long 'OFF' duration. In such ON-OFF dynamics and oxidation/antioxidation processes, the excitation light intensity plays a crucial role on the density and fate of charge-carriers. Apart from this, the confinement or diffusion of locally generated multiple charge-carriers depends upon the particle-particle interaction.
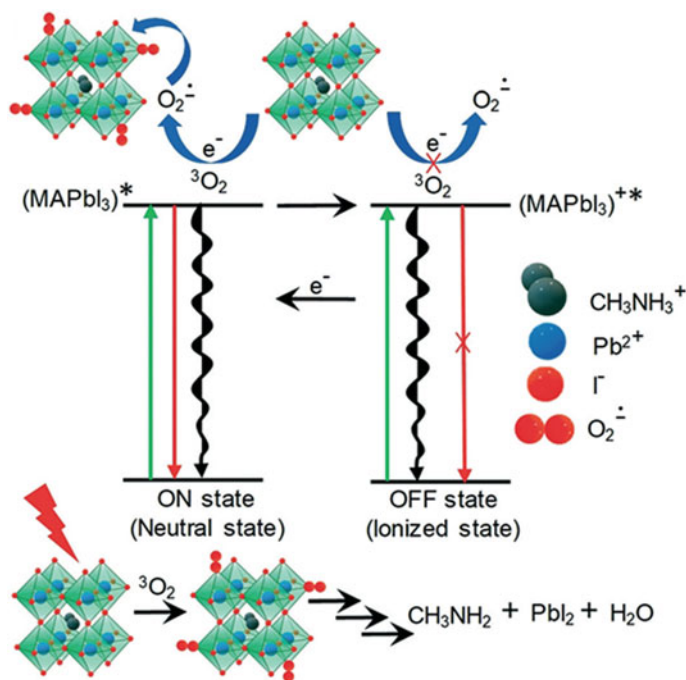
Fig. 11.4 Oxidation in perovskite. Schematic representation of the PL blinking and the degradation of the MAPbI₃ PNCs. Reproduced with permission from Ref. [25]. Copyright 2019, Wiley-VCH

11.4 Carrier Migration in Perovskite Assemblies

When semiconductor nanocrystals or QDs are assembled into a superlattice, their individual properties transform to produce more unique optical, electronic, and thermal properties. This arises from the interaction between the individual particles in the assembly [28–30]. In a superlattice, when the QDs are very close to each other, the interaction between their electronic wavefunctions increases. At a point, when the inter-particle spacing is too short, the discrete energy states of individual nanocrystals or QDs split to form minibands. As the result, long-range energy and charge transport in these superlattices through these bands become possible [30]. Strong electronic coupling and the formation of minibands as a function of inter-particle distance in semiconductor nanocrystal superlattice is shown schematically in Fig. 11.5. Such properties of QD superlattice are highly applicable in electronic, opto-electronic and thermoelectric devices [30, 31]. Since the pioneering work of Bawendi and coworkers on chalcogenide QD superlattices [28], many researchers have carried out a successful coupling of QDs and migration of energy or excitons among them in their two- or three-dimensional superlattice structures [31–33]. Exciton diffusion is observed in a highly ordered CdSe QD superlattice with center-to-center distance less than 7 nm between the adjacent QDs [32]. In such QD superlattices, the exciton
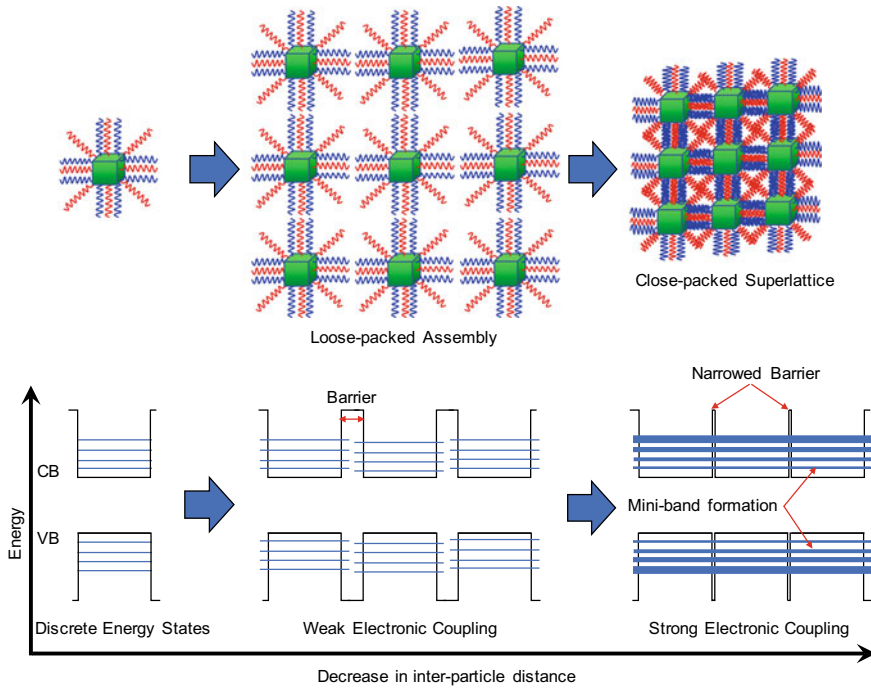
Fig. 11.5 Scheme showing strong electronic coupling and the formation of minibands in semiconductor nanocrystal superlattice

diffusion length as longer as 125 nm is reported. A faster exciton diffusion among highly interacting QDs can result in a faster exciton decay, which is attributed to the larger number of traps or defect sites on different QDs that the excitons may encounter within their lifetime. Besides, a highly ordered QD superlattice can result lower PLQY when compared to the disordered films and colloidal QD samples. This is ascribed to the faster energy transfer among closely-packed QDs. Similarly, directional transport of excitons is observed in long-range ordered and strongly coupled binary nanocrystal superlattice of PbSe consisting of two different sizes [33]. The surface-to-surface inter-particle spacing in such QD array can be reduced further by ligand exchange which results in the ultrafast exciton decay within few picoseconds, showing strong electronic coupling between QDs.

In a QD superlattice, the coupling energy between the individual QDs is much smaller than the exciton binding energy. Therefore, the excitons do not dissociate into free charge-carriers in the superlattice, rather they diffuse or hop and undergo ultrafast recombination, or the nonradiative energy transfer takes place among the closely-packed QDs. On the other hand, if the inter-particle distance between the QDs is very small (for example, center-to-center distance <1 nm), it induces sintering and straining of QDs, leading to increased disorder [29, 32]. Owing to these limitations of QD solids, a superlattice of semiconductor nanocrystals where long-range diffusion
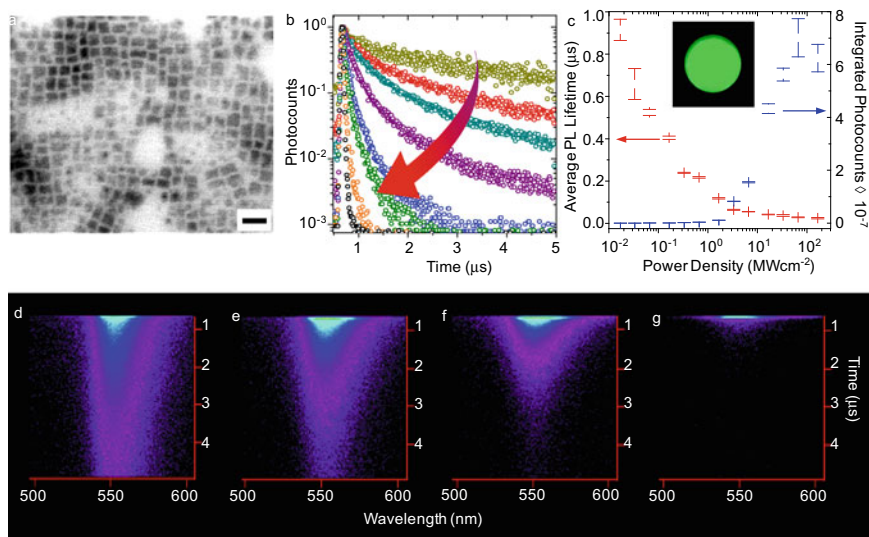
Fig. 11.6 Excitation intensity-dependent PL and charge-carrier properties of PNC films. **a** TEM image of MAPbBr$_3$ PNCs. The scale bar is 20 nm. **b** PL decay profiles of a MAPbBr$_3$ PNC film under increasing intensity of excitation laser: (top) 0.0175 to (bottom) 170 MWcm^{-2}. **c** Plots of the PL lifetime and the number of photons emitted as a function of excitation laser power for a MAPbBr$_3$ PNC film. Inset: MAPbBr$_3$ PNC film under UV light. **d–g** Temporally and spectrally resolved photocount maps of a FAPbBr$_3$ PNC film with an increase in excitation laser power: **d** 0.17, **e** 1.7, **f** 17, **g** 170 MWcm^{-2}. Reproduced with permission from Ref. [34]. Copyright 2019, American Chemical Society

of free charge-carriers, which is associated with delayed recombination, is largely required for their efficient applications in solar cells; and the organic-inorganic hybrid lead halide perovskites are promising candidates for this purpose.

Organic-inorganic hybrid PNCs (Fig. 11.6a) when assembled into close-packed film (Fig. 11.1c inset) show unexpectedly delayed PL (Fig. 11.6b, c, and d) under low-intensity excitation [34, 35], which are comparable to the free carrier recombination in single microcrystals and bulk films of perovskites [2, 3, 7, 14]. For instance, a PL lifetime >900 ns is observed for MAPbBr$_3$ PNC film [34], which becomes much longer (>4 μs) in the case of FAPbBr$_3$ (FA = formamidinium, CHN$_2$H$_3$$^+$) perovskite nanocrystal PNC film [35]. Under the increasing excitation intensity, the radiative recombination becomes extremely fast, resulting in amplified emission. The excitation intensity-dependent PL decay profiles of MAPbBr$_3$ PNC film and the temporally and spectrally resolved photocount maps of FAPbBr$_3$ PNC film are shown in Fig. 11.6b, and d–g, respectively. The fast PL lifetimes at higher intensities of excitation are associated with the exponential rise in the number of photons emitted by the PNC film, which is discussed in Fig. 11.6c. On the other hand, a fast PL is obvious in the case of isolated PNCs in their colloidal solution, irrespective of the intensity of excitation. These observations point toward the long-range migration of excitonically unbound charge-carriers at low-intensity excitation and spatial confinement of these

charge-carriers at higher intensities in PNC films. The amplified emission can be assigned to the radiative recombination of high-density electrons and holes that are generated and spatially confined among the close-packed PNCs in the film [34, 35].

The dynamics of charge-carriers generated in a PNC film at low- and high-intensity excitations is shown schematically in Fig. 11.7a and b, respectively. At high-intensity excitation, manifold charge-carriers are generated among different PNCs in the irradiated area (Fig. 11.7b). On the other hand, the concentration of photogenerated charge-carriers is less at low-intensity excitation, which reduces the carrier-carrier interactions and allows for the long-range diffusion in the film (Fig. 11.7a). Owing to such a long-range carrier diffusion, PNC films excited with low-intensity laser show
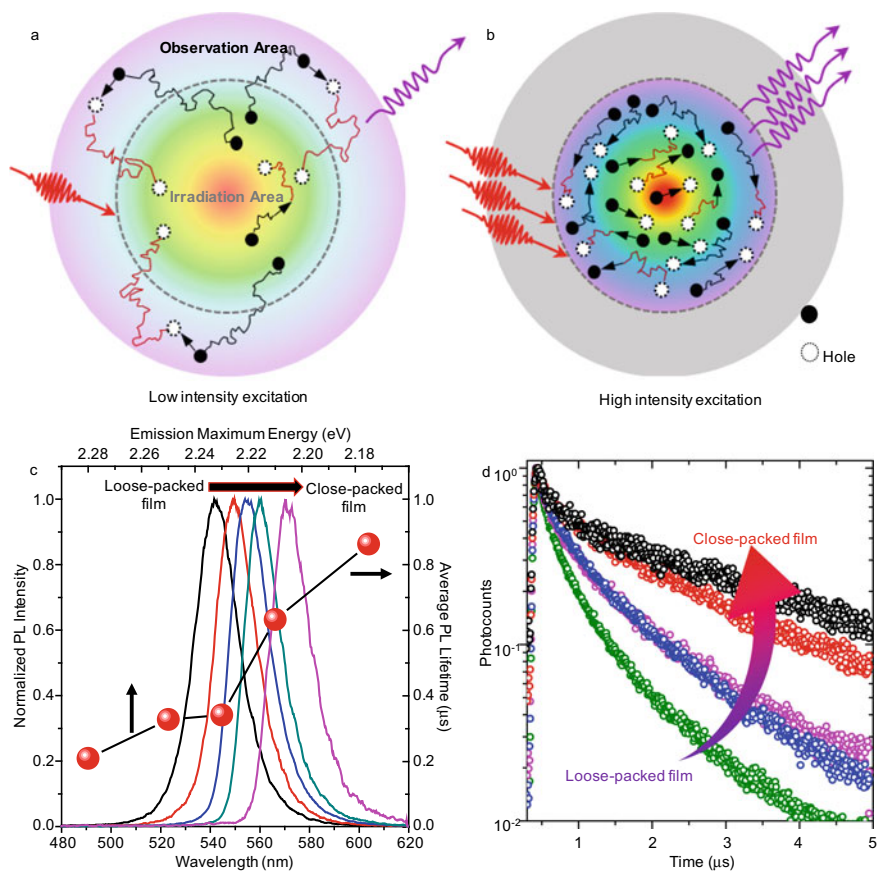
Fig. 11.7 Diffusion and recombination of charge-carriers in a PNC film **a**, **b** Scheme of charge-carrier diffusion and recombination in a PNC film under **a** low-intensity and **b** high-intensity excitations. **c** PL spectra of FAPbBr$_3$ PNC films with different PNC density. The corresponding PL lifetime values are shown in the line-symbol plot. **d** PL decay profiles of FAPbBr$_3$ PNC films with different PNC density. Reproduced with permission from Ref. [34]. Copyright 2019, American Chemical Society

Fig. 11.8 PL decay profiles of a PNC film excited with low-intensity laser (0.0175 μJ/pulse) (red) before and (blue) after doping with C_{60}. Reproduced with permission from Ref. [35]. Copyright 2019, Royal Society of Chemistry
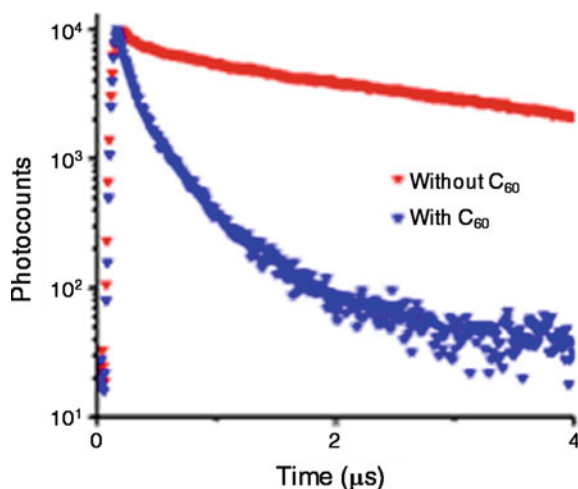
unexpectedly delayed PL. On the other hand, the diffusion of photogenerated charge-carriers is spatially confined by increasing the intensity of excitation laser, which is the result of an increase in the carrier concentration. Accordingly, the rate of radiative recombination within the irradiated area controls over the diffusion, providing amplified emission.

The degree of charge-carrier migration across PNCs in their close-packed assembly (or film) depends upon their packing density [34]. As seen in Fig. 11.7c, the PL spectra of a loose-packed PNC film is blue-shifted, whereas that of a close-packed film is red-shifted. Additionally, as shown in Fig. 11.7c and d, a red-shifted PL spectrum is associated with long PL lifetime. The low-energy photons which are associated with the delayed emission in PNC film point toward the diffusion of charge-carriers through closely-spaced energy states during which some energy is lost, resulting in long-lived low-energy photons. Such delayed PL, as a result of long-range migration of photogenerated charge-carriers, in close-packed assembly of PNCs is a promising property for the harvesting of charge-carriers in high-efficiency solar cells. Indeed, an appreciable rate of electron transfer $(3.3 \times 10^6 \text{ s}^{-1})$ is achieved from the photoexcited close-packed assembly of PNCs to fullerene (C_{60}), revealed by the fast PL decay of the PNC film doped with C_{60}, when compared to a pristine film without C_{60}, as shown in Fig. 11.8 [35].

11.5   Conclusions

The optical and electronic properties of individual QDs modify when they are arranged into superlattices. The overlapping of QDs electronic wavefunctions in the lattice facilitates the long-range diffusion or hopping of excitons. Due to the high exciton binding energy in strongly quantum-confined systems, the diffusing excitons

do not dissociate into free charge-carriers. Thus, the exciton recombination becomes ultrafast, and the isolated semiconductor nanocrystals or QDs show PL blinking. In contrast, metal halide perovskite nanocrystals and QDs arranged into superlattices exhibit long-range carrier migration and delayed radiative recombination. This is analogous to the long-range diffusion of free charge-carriers in bulk perovskites, suggesting a weak confinement of photogenerated electron-hole pairs. The formation of new inter-particle energy states in superlattices of PNCs assist in the diffusion of coulombically uncorrelated electrons and holes. Such freely diffusing electrons are effectively harvested using C_{60}. Therefore, superlattices of PNCs are promising structures for the development of high-efficiency solar cells.

References

1. Kojima A, Teshima K, Shirai Y, Miyasaka T (2009) Organometal halide perovskites as visible-light sensitizers for photovoltaic cells. J Am Chem Soc 131:6050–6051
2. Dong Q, Fang NY, Shao Y, Mulligan P, Qiu J, Cao L, Huang J (2015) Electron-hole diffusion lengths > 175 μm in solution-grown $CH_3NH_3PbI_3$ single crystals. Science 347:967–970
3. deQuilettes DW, Vorpahl SM, Stranks SD, Nagaoka H, Eperon GE, Ziffer ME, Snaith HJ, Ginger DS (2015) Impact of microstructure on local carrier lifetime in perovskite solar cells. Science 348:683–686
4. Zhang F, Zhong H, Chen C, Wu X, Hu X, Huang H, Han J, Zou B, Dong Y (2015) Brightly luminescent and color-tunable colloidal $CH_3NH_3PbX_3$ (X = Br, I, Cl) quantum dots: potential alternatives for display technology. ACS Nano 9:4533–4542
5. Kim Y-H, Cho H, Heo JH, Kim T-S, Myoung N, Lee C-L, Im SH, Lee T-W (2015) Multicolored organic/inorganic hybrid perovskite light-emitting diodes. Adv Mater 27:1248–1254
6. Yakunin S, Protesescu L, Krieg F, Bodnarchuk MI, Nedelcu G, Humer M, De Luca G, Fiebig M, Heiss W, Kovalenko MV (2015) Low-threshold amplified spontaneous emission and lasing from colloidal nanocrystals of caesium lead halide perovskites. Nat Commun 6:8056
7. Saba M, Cadelano M, Marongiu D, Chen F, Sarritzu V, Sestu N, Figus C, Aresti M, Piras R, Lehmann AG, Cannas C, Musinu A, Quochi F, Mura A, Bongiovanni G (2014) Correlated electron-hole plasma in organometal perovskites. Nat Commun 5:5049
8. Yang Y, Yang M, Li Z, Crisp R, Zhu K, Beard MC (2015) Comparison of recombination dynamics in $CH_3NH_3PbBr_3$ and $CH_3NH_3PbI_3$ perovskite films: influence of exciton binding energy. J Phys Chem Lett 6:4688–4692
9. Jha A, Duan H-G, Tiwari T, Nayak PK, Snaith HJ, Thorwart M, Miller RJD (2018) Direct observation of ultrafast exciton dissociation in lead iodide perovskite by 2D electronic spectroscopy. ACS Photonics 5:852–860
10. Phuong LQ, Yamada Y, Nagai M, Maruyama N, Wakamiya A, Kanemitsu Y (2016) Free carriers versus excitons in $CH_3NH_3PbI_3$ perovskite thin films at low temperatures: charge transfer from the orthorhombic phase to the tetragonal phase. J Phys Chem Lett 7:2316–2321
11. Blancon J-C, Tsai H, Nie W, Stoumpos CC, Pedesseau L, Katan C, Kepenekian M, Soe CMM, Appavoo K, Sfeir MY, Tretiak S, Ajayan PM, Kanatzidis MG, Even J, Crochet JJ, Mohite AD (2017) Extremely efficient internal exciton dissociation through edge states in layered 2D perovskites. Science 355:1288–1292

12. Miyata A, Mitioglu A, Plochocka P, Portugall O, Wang JT, Stranks SD, Snaith HJ, Nicholas RJ (2015) Direct measurement of the exciton binding energy and effective masses for charge carriers in organic-inorganic tri-halide perovskites. Nat Phys 11:582–587

13. Butkus J, Vashishtha P, Chen K, Gallaher JK, Prasad SKK, Metin DZ, Laufersky G, Gaston N, Halpert JE, Hodgkiss JM (2017) The Evolution of quantum confinement in $CsPbBr_3$ perovskite nanocrystals. Chem Mater 29:3644–3652

14. Shi D, Adinolfi V, Comin R, Yuan M, Alarousu E, Buin A, Chen Y, Hoogland S, Rothenberger A, Katsiev K, Losovyj Y, Zhang X, Dowben PA, Mohammed OF, Sargent EH, Bakr OM (2015) Low trap-state density and long carrier diffusion in organolead trihalide perovskite single crystals. Science 347:519–522

15. Levchuk I, Osvet A, Tang X, Brandl M, Perea JD, Hoegl F, Matt GJ, Hock R, Batentschuk M, Brabec CJ (2017) Brightly luminescent and color-tunable formamidinium lead halide perovskite $FAPbX_3$ (X = Cl, Br, I) colloidal nanocrystals. Nano Lett 17:2765–2770

16. Zheng K, Zhu Q, Abdellah M, Messing ME, Zhang W, Generalov A, Niu Y, Ribaud L, Canton SE, Pullerits T (2015) Exciton binding energy and the nature of emissive states in organometal halide perovskites. J Phys Chem Lett 6:2969–2975

17. Li M, Bhaumik S, Goh TW, Kumar MS, Yantara N, Grätzel M, Mhaisalkar S, Mathews N, Sum TC (2017) Slow cooling and highly efficient extraction of hot carriers in colloidal perovskite nanocrystals. Nat Commun 8:14350

18. Li M, Begum R, Fu J, Xu Q, Koh TM, Veldhuis SA, Grätzel M, Mathews N, Mhaisalkar S, Sum TC (2018) Low threshold and efficient multiple exciton generation in halide perovskite nanocrystals. Nat Commun 9:4197

19. Tanaka K, Takahashi T, Ban T, Kondo T, Uchida K, Miura N (2003) Comparative study on the excitons in lead-halide-based perovskite-type crystals $CH_3NH_3PbBr_3$ $CH_3NH_3PbI_3$. Solid State Commun 127:619–623

20. Ghimire S, Biju V (2018) Relations of exciton dynamics in quantum dots to photoluminescence, lasing, and energy harvesting. J Photochem Photobiol C 34:137–151

21. Galland C, Ghosh Y, Steinbrück A, Sykora M, Hollingsworth JA, Klimov VI, Htoon H (2011) Two types of luminescence blinking revealed by spectroelectrochemistry of single quantum dots. Nature 479:203–207

22. Tian Y, Merdasa A, Peter M, Abdellah M, Zheng K, Ponseca CS Jr, Pullerits T, Yartsev A, Sundström V, Scheblykin IG (2015) Giant photoluminescence blinking of perovskite nanocrystals reveals single-trap control of luminescence. Nano Lett 15:1603–1608

23. Gerhard M, Louis B, Camacho R, Merdasa A, Li J, Kiligaridis A, Dobrovolsky A, Hofkens J, Scheblykin IG (2019) Microscopic insight into nonradiative decay in perovskite semiconductors from temperature-dependent luminescence blinking. Nat Commun 10:1698

24. Park Y-S, Guo S, Makarov NS, Klimov VI (2015) Room temperature single-photon emission from individual perovskite quantum dots. ACS Nano 9:10386–10393

25. Chouhan L, Ghimire S, Biju V (2019) Blinking beats bleaching: the control of superoxide generation by photo-ionized perovskite nanocrystals. Angew Chem Int Ed 58:4875–4879

26. Li C, Zhong Y, Luna CAM, Unger T, Deichsel K, Gräser A, Köhler J, Köhler A, Hildner R, Huettner S (2016) Emission enhancement and intermittency in polycrystalline organolead halide perovskite films. Molecules 21:1081

27. Yuan G, Ritchie C, Ritter M, Murphy S, Gómez DE, Mulvaney P (2018) The degradation and blinking of single $CsPbI_3$ perovskite quantum dots. J Phys Chem C 122:13407–13415

28. Murray CB, Kagan CR, Bawendi MG (1995) Self-organization of CdSe nanocrystallites into three-dimensional quantum dot superlattices. Science 270:1335–1338

29. Collier CP, Vossmeyer T, Heath JR (1998) Nanocrystal superlattices. Annu Rev Phys Chem 49:371–404

30. Kagan CR, Murray CB (2015) Charge transport in strongly coupled quantum dot solids. Nat Nanotechnol 10:1013–1026

31. Harman TC, Taylor PJ, Walsh MP, LaForge BE (2002) Quantum dot superlattice thermoelectric materials and devices. Science 297:2229–2232

32. Yoon SJ, Guo Z, dos Santos Claro PC, Shevchenko EV, Huang L (2016) Direct imaging of long-range exciton transport in quantum dot superlattices by ultrafast microscopy. ACS Nano 10:7208–7215
33. Wu Y, Li S, Gogotsi N, Zhao T, Fleury B, Kagan CR, Murray CB, Baxter JB (2017) Directional carrier transfer in strongly coupled binary nanocrystal superlattice films formed by assembly and *in situ* ligand exchange at a liquid-air interface. J Phys Chem C 121:4146–4157
34. Ghimire S, Chouhan L, Takano Y, Takahashi K, Nakamura T, Yuyama K, Biju V (2019) Amplified and multicolor emission from films and interfacial layers of lead halide perovskite nanocrystals. ACS Energy Lett. 4:133–141
35. Ghimire S, Nair VC, Muthu C, Yuyama K, Vacha M, Biju V (2019) Photoinduced photoluminescence enhancement in self-assembled clusters of formamidinium lead bromide perovskite nanocrystals. Nanoscale 11:9335–9340